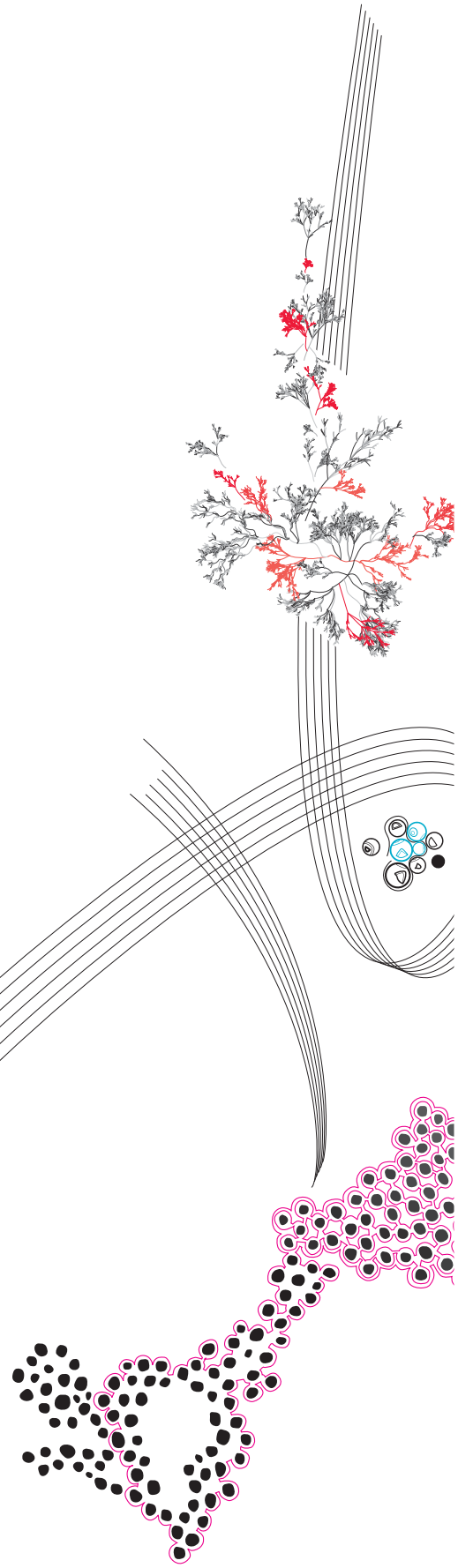

BSc Thesis Biomedical Technology

Comparison of different meshing methods regarding the electric field simulations of deep brain stimulation

Thomas J. Martens

July, 2024

Supervisor: dr.ir. B.C. Schwab
External supervisor: dr.rer.nat. M.C. Piastra
Daily Supervisor: T. Keizers MSc

Department of Biomedical Signals and Systems
Faculty of Electrical Engineering,
Mathematics and Computer Science

UNIVERSITY OF TWENTE.

Abstract

This thesis evaluates meshing problems that occur when generating a volumetric mesh of an electrode inside a brain for deep brain stimulation. A new robust meshing procedure is introduced to circumvent these problems. This procedure is able to robustly and accurately combine electrode-brain meshes.

The influence on the electric field when simulating deep brain stimulation is compared to different preexisting mesh generation procedures. The methods considered are: meshing only the electrode contacts within the brain (method 1), using domain relabelling to define electrode insulation (method 2), and the newly introduced procedure (method 3).

The new meshing procedure showed more mesh generation flexibility, making it possible to orient the electrode arbitrarily inside a domain. The difference in the electric fields between methods 2 and 3 was less pronounced. Still, it is recommended to use the new meshing procedure in future simulations to account for inter-patient variability in electrode placement.

Keywords: Parkinson's Disease, DBS, Simulation, Mesh, Electrode, Insulation

Contents

1 Introduction **2**

2 Problem Analysis **3**

3 Methods **5**
3.1 Mesh generation 5
3.2 Simulations 8

4 Results **10**
4.1 Mesh generation 10
4.2 Simulations 13

5 Discussion **20**

6 Conclusion **23**

References **25**

Appendix **27**

A Simulation Parameters **27**

1 Introduction

Parkinson's disease (PD) is the most common movement disorder and second most prevalent neurodegenerative disorder, affecting 1-2 in 1000 of the global population at any given time [1]. Parkinson's is diagnosed if a patient suffers from trouble with the initiation of voluntary movement (bradykinesia) in combination with one of the following symptoms: postural instability, muscular rigidity, or resting tremor [2].

Pathophysiology of Parkinson's

In PD, the region of interest is the basal ganglia. This region is central in coordinating voluntary movement and filtering out spontaneous brain activity [3].
In PD the dopaminergic neurons in the substantia nigra pars compacta (SNc) degenerate. This decreases the amount of dopamine released in the striatum, indirectly influencing the coordination of voluntary movement [3], as depicted in figure 1.

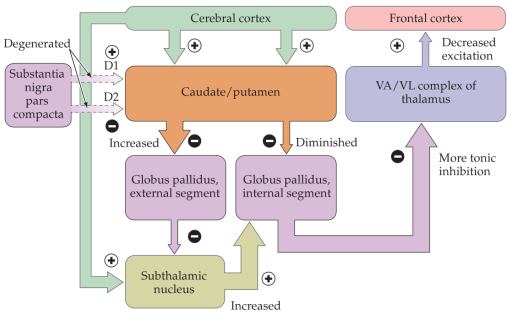

Figure 1: Schematic overview of the influence of degeneration of the SNc in PD. Figure taken from [4]

Currently, no treatments to cure Parkinson's disease exist. Although promising new gene therapy technologies are in clinical trials, most PD therapeutics currently focus on reducing symptoms [5]. PD patients are most often treated with pharmaceuticals to restore dopamine regulation in the brain. Depending on the symptoms, different classes of drugs are prescribed. The most common and most effective is Levodopa, a precursor to dopamine. However, when side effects worsen, or if efficacy weakens, deep brain stimulation (DBS) is an established alternative [5].

Deep Brain Stimulation

DBS is an invasive procedure where electrodes are placed directly inside the brain. Due to the invasivity and possible side effects, DBS is only applied in 2% of PD patients [6]. The electrodes are placed to stimulate specific targets within the basal ganglia, reducing the symptoms of the patient. The most common targets [7] are the subthalamic nucleus (STN) and the globus pallidus internus (GPI). These regions are empirically found to be the most effective in reducing symptoms. However, the exact working mechanisms of DBS are not yet known.

The leading theory on the mode of action is that the electrode modulates the brain activity by the local stimulation of brain regions directly around the electrode [8]. New evidence in the field of transcranial alternating current stimulation (tACS) suggests that weak electric fields (around 0.2V/m) can modulate neuron spike timings and influence synchronisation

in the motor cortex, reducing PD symptom severity [9, 10]. This begs the question if weak electric fields reaching the cortex during DBS influence the efficacy of the treatment.

The DECODE project aims to shed light on the interactions of these weak electric fields (E-fields) inside the cortical regions of the brain. This is done by first carrying out computer simulations of DBS, followed by comparison with patient data. This way, it is investigated if there is a correlation between simulated electric field strengths in the cortical regions and the symptom severity of the patient.

Simulation of DBS

For the simulations, the finite element method (FEM) is used to compute the electric fields inside the head. For FEM, the simulation domain is decomposed into smaller elements, the so-called mesh. By evaluating the partial differential equations for each separate element, the solution to the E-fields inside the brain can easily be obtained numerically [11]. The solution is found by the set of partial differential equations (in this case Maxwell's) and the boundary conditions set by the domain. To solve for the electric field, different pipelines exist. In the DECODE project, the FEMfuns [12] pipeline is used. In this thesis, however, COMSOL Multiphysics [13] is used. FEMfuns is primarily focused on the simulation of E-fields inside the head, whereas COMSOL has a general focus on solving a wide variation of equations. Both pipelines have been used and proven similar in calculating the electric fields during DBS [14].

Mesh generation

As explained in the previous section, a volumetric mesh, often decomposed in tetrahedrons, is needed to perform FEM simulations. For the simulation of DBS, the mesh should contain two parts: the whole head model and the electrode model.

SimNIBS [15] is a common tool for the simulation of non-invasive brain stimulation. Within SimNIBS it is possible to obtain a surface mesh of the head by segmentation of MRI images [16]. The electrode geometries and positions are obtained via the LeadDBS [17] MATLAB toolbox.

Both separate surface meshes should then be merged and transformed from a surface mesh to a volumetric mesh. This can be done via the Iso2Mesh [18] MATLAB toolbox. Iso2Mesh is a toolbox specifically designed to extract surface meshes from volumetric binary images and to post-process these meshes. This last functionality is primarily used in this thesis. Within Iso2Mesh, it should be possible to combine the electrode and the brain meshes and generate the volumetric mesh needed for the simulations.

2 Problem Analysis

The problem that is addressed in this thesis concerns the mesh generation of the combined electrode-brain mesh. During the DECODE project, it was found that two cases would lead the mesh generation to fail. The first one happens when the electrode lead pierces through another surface, i.e. when the electrode lead goes through the boundary between white and grey matter. The second case, and expectedly more severe, happens when electrode insulation is included in the model. Electric insulation restricts electric current and thus influences electric field propagation. Since it is currently not possible to correctly model

the insulation, it is expected that this negatively affects the simulation results within the DECODE project.

The cause of these problems lies within the surface-to-volumetric mesh generation. Iso2Mesh calls an external application, TetGen [19], to generate the tetrahedral mesh. TetGen uses a Delauney-based algorithm to generate the mesh. This algorithm assumes that the input surface is a piecewise linear complex (PLC). Piecewise linear complexes are structures that are a linear combination of sub-geometries. These complexes may contain internal boundaries, holes, and even unconnected lines, but must be watertight (figure 2a). What is not possible, is a geometry where two surfaces intersect without a proper boundary definition at the crossing, so-called self-intersections (figure 2b).

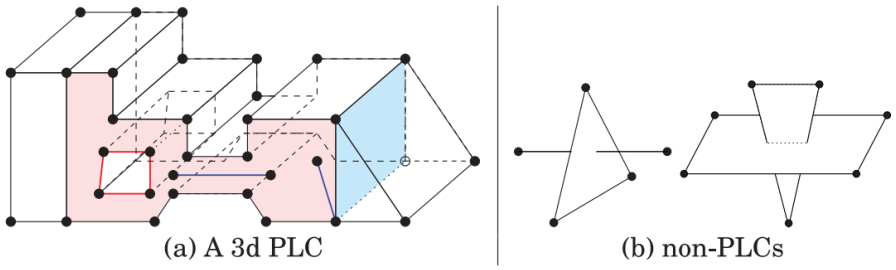

Figure 2: Two possible 3d geometries a) a PLC geometry and thus valid for TetGen, b) non-PLC geometry and thus invalid for TetGen. Figure taken from [19]

The two problematic cases described above have the same origin. When the electrode mesh and brain mesh are merged, the input surface for TetGen becomes a non-PLC geometry. Causing the mesh generation to fail.

A MATLAB function written by Thomas Keizers makes it still possible to introduce electrode insulation into the mesh, but using this function alters the insulation geometry severely. With this function, the first problematic case, when the electrode pierces a boundary, still exists. This makes this method not an ideal solution. This is why simulations within the DECODE project are currently carried out with only the electrode contacts.

This thesis will introduce a new method to merge the electrode and the brain meshes and will discuss the difference between the different methods regarding the simulation of DBS.

Research question

What is the influence of using different methods for meshing the insulation of an electrode on the electric fields during the simulation of deep drain stimulation using the finite element method?

Subquestion

Is it possible to find a method to introduce the whole electrode into the brain mesh, such that electrode geometry is conserved?

3 Methods

This thesis is split into two parts. The first part focuses on the mesh generation of the combined electrode-brain mesh. The second part focuses on the resulting simulations to find the difference between these meshing methods. For this thesis, two hardware sources were used. The primary hardware source had the following hardware specifications: CPU: Intel(R) CORE(TM) i7-10750H @ 2.60GHz, RAM: 16GB, GPU: NVIDIA Quadro T1000. The secondary hardware source used had the following: CPU: Intel(R) Xeon(R) Gold 5218 @ 2.30GHz, RAM: 191GB, (GPU: not specified).

3.1 Mesh generation

Three different mesh generation methods are used. These methods aim to merge the electrode into another, arbitrary, domain. Mesh generations were done using the Iso2Mesh [18] toolbox in MATLAB on the primary hardware source. The first method is used as a baseline in which only the electrode contacts are introduced to the domain. The DECODE project currently uses this first method for the whole head simulations. The second method is a 'work-around' method based on a function that relabels domain elements to insulation, written by Thomas Keizers. The third method is newly developed in this thesis and introduces the whole electrode with conserved surface geometry.

The electrode geometry used in this thesis is the Medtronic 3389 DBS lead, imported from the Lead-DBS [17] MATLAB toolbox (figure 3). The electrode geometry is separated into 9 different subdomains. Four of these correspond to electrode contacts (numbers 0 to 3 in the figure), and the remaining light-grey areas correspond to the insulation of the DBS lead. For the mesh generation, the default electrode position is chosen to be aligned with the z-axis, with the middle point of the contacts centred at (x,y,z) = (0,0,0). In the following subsections, the working mechanisms of the three different methods are discussed.

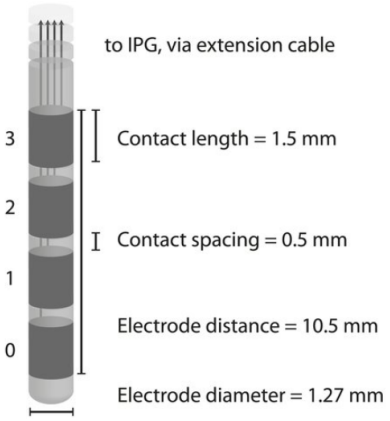

Figure 3: The Medtronic 3389 DBS lead, numbers 0 to 3 represent the electrode contacts, and the light grey areas indicate electrode insulation. Figure taken from [20]

Method 1

In method 1, first, the electrode domains corresponding to the contacts are imported and merged with the spherical domain. Since there are no intersecting surfaces, this merged mesh does not need to be processed further and the volumetric mesh is generated using the *surf2mesh* function (Iso2Mesh). The mesh is finally exported to a suitable file format for simulation: .mphtxt for the COMSOL pipeline, and .msh for the FEMfuns pipeline.

Algorithm 1: Method 1

Result: Volumetric mesh with only contacts of electrode

```
Import electrode submeshes;
Define/import domain to merge into;
Centre electrode and align to z-axis;
for Electrode contact submeshes do
    Concatenate submeshes to new full electrode mesh;
end
Translate and rotate electrode to arbitrary position;
for All meshes do
    Find internal point for surf2mesh domain generation;
end
for All meshes do
    Merge meshes into one;
end
Generate volumetric mesh;
```

Method 2

Method 2 consists of the same steps as method 1
and introduces a post-processing step. After the volumetric mesh generation, a relabelling function is called. This function evaluates all coordinates where the electrode would be inside the domain, and checks if the centroids of the domain elements would lie inside the reference subdomain of the electrode from LeadDBS. If it does, it relabels the element to the specific domain corresponding to the electrode part, e.g. insulation in between contact 1 and 2, or the electrode tip.

Algorithm 2: Relabel function

Result: Volumetric mesh with domains correctly labelled

```
Define domain labels to keep;
Define submesh to check and relabel to;
Define minimum and maximum coordinates to check (confined around electrode);
for All coordinates to check do
    Calculate centroids;
end
if Centroids in submesh then
    if element not in labels to keep then
        Relabel element to submesh;
    end
end
```

During mesh generation, the relabel function was identified as a bottleneck in efficiency. The code was rewritten to make use of MATLAB's high efficiency of logical matrix operations. With logical indexing, the post-processing time was reduced by 85% for a homogeneous spherical domain (radius=70mm).

Method 3

Method 3 is based on the relabelling function. This method introduces extra pre- and post-processing steps to conserve the electrode geometry and to make it possible to have the electrode cross a boundary of a domain without self-intersections.

Algorithm 3: Method 3

Result: Volumetric mesh, obtained from brain and electrode surface meshes

```
Import electrode submeshes;
Define/import domain to merge into;
Centre electrode and align to z-axis;
for All electrode sub meshes do
    Concatenate submeshes to new mesh;
end
Refine new electrode mesh;
(opt. Refine domain meshes;)
Translate and rotate electrode to arbitrary position;
for All meshes do
    Find internal point for surf2mesh domain generation;
end
for Merge meshes into one;
 do All meshes
end
Generate volumetric mesh;
Relabel volumetric mesh;
while There are conflicting domains do
    Check for conflicting elements;
    Find neighbours of conflicting elements;
    for Conflicting elements do
        if Any neighbour not conflicting then
            Relabel conflicting elements to the closest non-conflicting neighbour
        end
    end
end
```

First, all electrode parts are imported and concatenated, resulting in all 9 electrode subdomains being in the same mesh. To remove the overlapping boundaries between parts, the *remeshsurf* function (Iso2Mesh) is called. This function does two essential things for this method. It refines the surface mesh of the electrode, resulting in the more precise geometry needed to merge the electrode in another domain without self-intersections. Secondly, it removes all internal boundaries of the concatenated electrode parts. This results in a self-intersection-free electrode mesh consisting of only one domain.

After the remeshing, the electrode surface is merged with the other surface mesh (e.g. brain) using the *surfboolean* function (Iso2Mesh). The merged mesh is used as input for *surf2mesh* (Iso2Mesh) to create the volumetric mesh. This mesh is then again relabelled via algorithm 2. Since we included the whole electrode geometry to generate the volumetric mesh, the mesh elements are generated such that the geometry should be conserved during the relabelling.

Finally, corrections to the relabelling of the electrode should be done. The relabelling works by comparing elements to the originally imported electrode, however, since our electrode has been remeshed, these do not agree with each other. This causes elements of the electrode to not be labelled as such. This is resolved by checking all conflicting elements for their neighbouring domains, after which the conflicting element acquires the closest electrode subdomain.

Mesh Testing

To test the properties of the different mesh generation methods, the merging of the electrode in different domains was tested. To test the properties of the electrode for a method, a spherical domain with a radius of 70mm was used. The electrode contacts and sphere were centred at (x,y,z)=(0,0,0).

To test if method 3 succeded in robust mesh generation, the electrode was merged with different orientations in different geometrical domains. This way it could be analysed if method 3 would run into the same problems as defined in the problem analysis. The first was a case where the electrode crosses a corner of a box, the second was a case where the electrode pierces the surface of a spherical domain, and the third was where the electrode was inserted into the Ernie brain model (SimNIBS [15]), consisting of white matter and grey matter.

3.2 Simulations

The simulations in this thesis were carried out in COMSOL Multiphysics [13]. The electric currents (ec) module was used and evaluated for a stationary study. To run COMSOL, the secondary hardware source was used.

The influence of the different meshing methods was tested with two main simulation scenarios. The first scenario compared the three meshing methods on their influence on the E-field by simulating a homogeneous spherical model (figure 4a). The second scenario compared the first and the third meshing methods in a simplified head model to see if there would be a difference when simulating a model with different conductivities, which is relevant for the DECODE project (figure 4b). In all simulation scenarios, both monopolar and bipolar stimulation settings were used. The material properties and simulation parameters can be found in appendix A.

For the first simulation scenario, the three meshes were generated in MATLAB and exported to a .mphtxt file, which could be imported into COMSOL. After the meshes were imported, materials and boundary conditions were applied.

The mesh generation for the second scenario was done in COMSOL itself. Importing errors were caused in COMSOL due to the volumetric mesh generation in Iso2Mesh removing boundary labels. This made it not possible to use Iso2Mesh for the scenario.

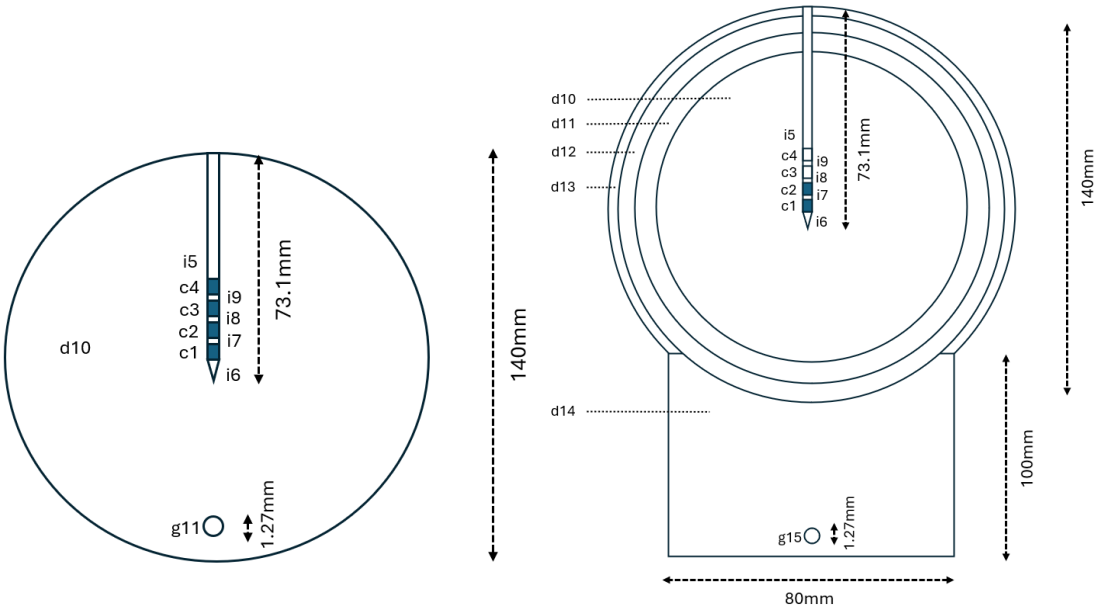

Figure 4: Schematic representations of the domains used in the simulation scenarios. a) scenario 1, b) scenario 2

Analysis of the electric fields

The electric field and electric potential on the xz-, xy-, and yz-planes were exported to MATLAB to analyse simulation results. In MATLAB, the data was first processed. The data at the mesh nodes was interpolated to an equidistant grid with a resolution of 0.05mm. This made it possible to compare the different simulations with each other. With the help of the electric potential in a plane and the resulting E-field, plots were made to indicate the magnitude and direction of the E-field. To compare between methods, the relative difference in electric field magnitude was calculated for methods within the same scenario. The resulting plots show increases or decreases in E-field magnitude.

To further quantify this data, the difference in E-field magnitude between methods was extracted from the 2D plots by evaluating the relative difference at a specific radius from the centre of the electrode contacts. This data was plotted by evaluating the relative difference in E-field magnitude at a specific distance from the contacts as a function of the angle in the domain. Using the assumption that the domain is axisymmetric, it was chosen to focus on the xz-plane for the data analysis and to only evaluate half of the domain (0°-180°). 0°corresponds to the angle towards the electrode stem and 180°corresponds to the angle towards the electrode tip (figure 5).

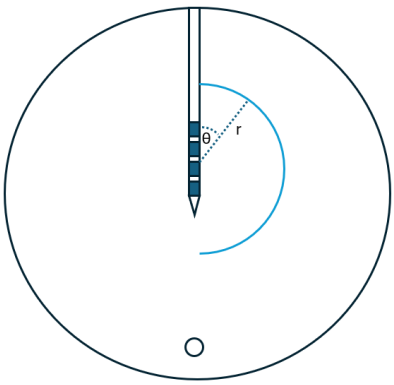

Figure 5: An example of along which line the data is transformed to analyse the relative difference in E-field magnitude.

To show the influence of different meshing methods on the locality of influences in a domain, the

absolute peak sizes of the line plots were calculated. The peak size was calculated by taking the absolute difference of the maximum and minimum values at a specific distance from the electrode. If this peak size is small, it indicates that the difference in the E-field is even around the domain at a specific distance. If the peak size is large, it indicates the existence of local areas in the domain where the difference in E-field magnitude is more prominent compared to other areas.

4 Results

In this section, mesh performance and simulation results will be shown.

4.1 Mesh generation

Figure 6 shows the electrode leads resulting from each meshing method. Method 1 produces the contacts with preserved geometry and no insulation. Method 2 has four electrode contacts with preserved geometry. The insulation regions have low, inconsistent resolution. In between the contacts, the resolution of the insulation is higher than in the stem. Method 3 introduces both the contacts and the insulation of the electrode in the same resolution. We do see that the contacts and insulation are not exactly preserving the reference geometry: the surface becomes less even. This is seen when comparing the electrode contacts between different methods. The influence on the internal and outer boundaries can be seen in figure 7. This figure shows one contact and one neighbouring insulation region. After remeshing, the geometry still represents the contact, but the resolution is lower, especially on the internal boundaries between electrode contacts (figure 7c). However, the electrode's outer surface has a more consistent resolution over the whole lead than method 2.

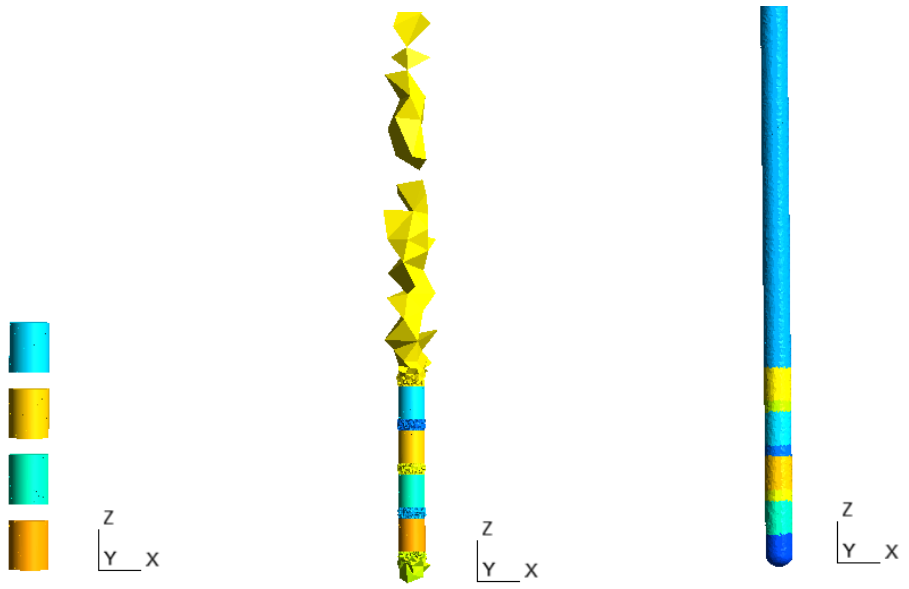

(a) **(b)** **(c)**

Figure 6: Electrode mesh and subdomains indicated by colour by the different meshing methods a) meshing method 1, b) meshing method 2, c) meshing method 3.

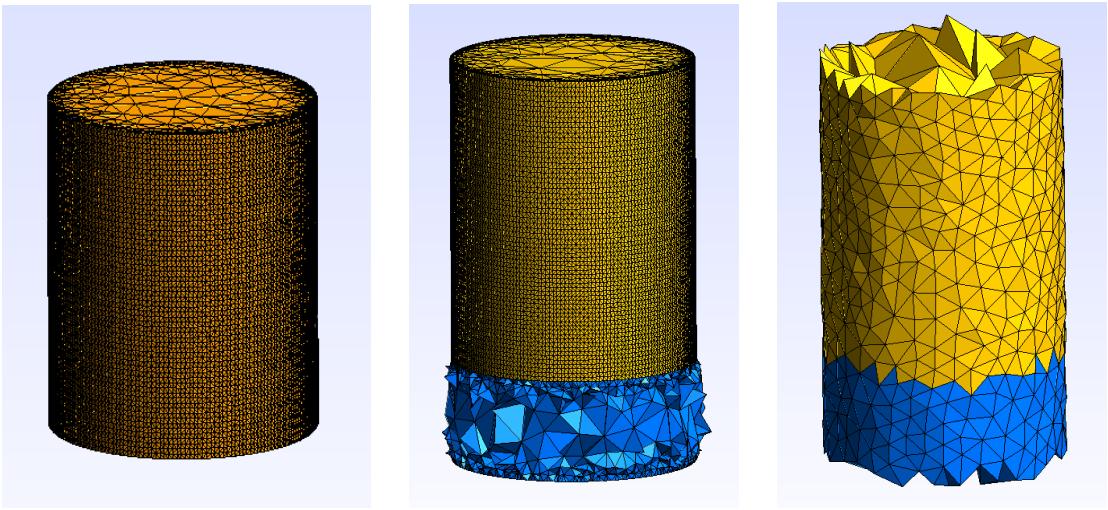

(a) **(b)** **(c)**

Figure 7: Electrode mesh showing an internal boundary (on top) and the outer boundary, evaluated for one contact and one insulation domain a) meshing method 1, b) meshing method 2, c) meshing method 3.

The different meshes generated to test the capabilities of the third meshing method can be seen in figure 8. Method 3 can handle the different orientations and the different domains correctly. It is still able to define the different subdomains correctly and conserve the electrode geometry. It is important to note here that the remeshing settings during the mesh generation might need to be changed per domain. It was found that complex domains, such as the whole brain, or more complex orientations, such as partly piercing the side of a sphere, needed higher refinements before merging with the electrode mesh. Both the electrode and non-electrode domains needed sufficient refinement to produce self-intersection-free meshes.

For the refinement of the brain mesh, significantly more RAM (around 25GB) was needed than available on the primary hardware source. Therefore it was needed to run this specific mesh on the secondary hardware source.

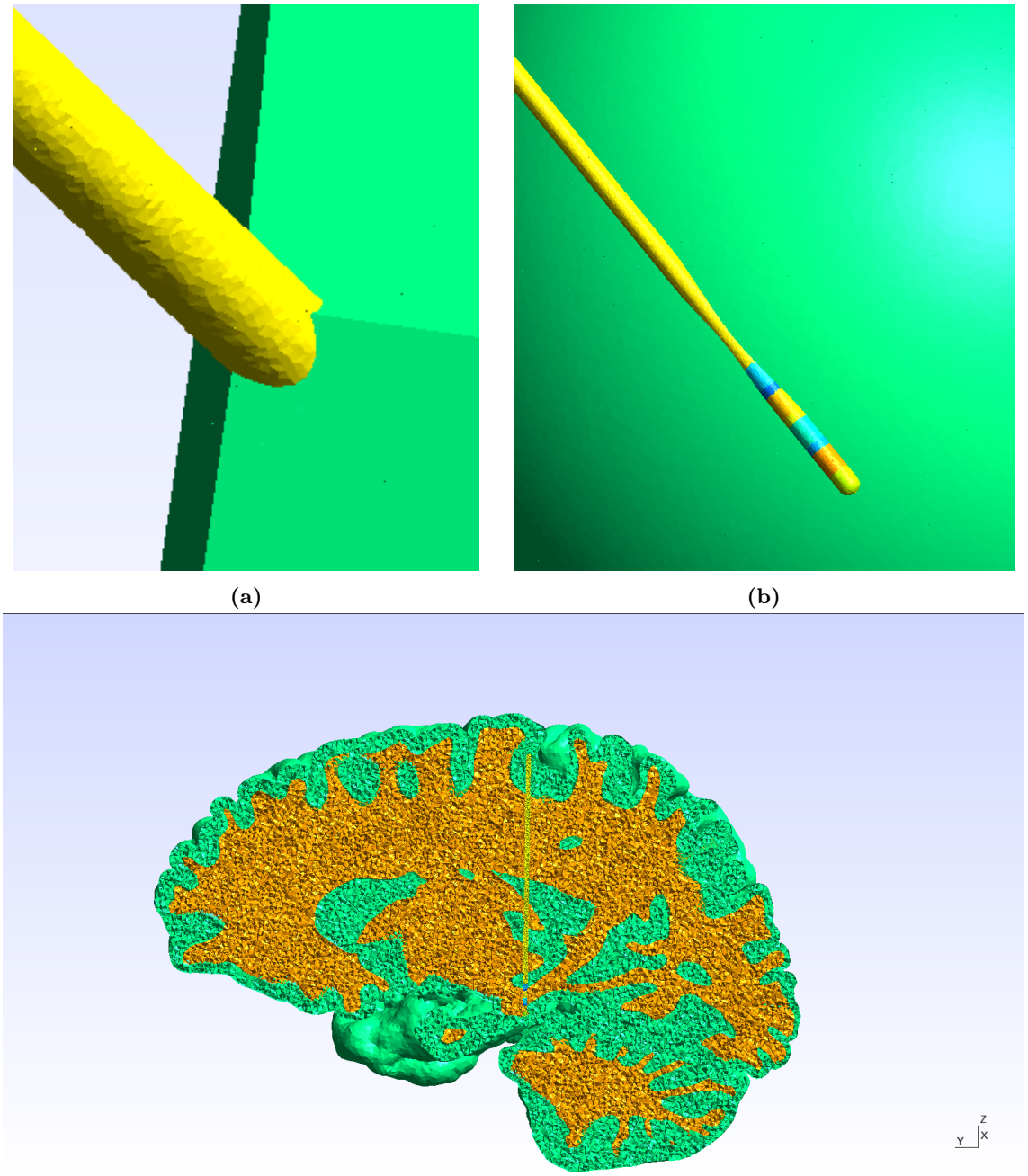

Figure 8: Meshes generated by method 3, testing different domains and orientations, the used parameter value for the refinement via the *remeshsurf* function are specified in the brackets a) electrode piercing corner of a box. (electrode: 0.1, domain: 2), b) electrode piercing surface of a sphere (electrode: 0.1, domain: 2), c) electrode inside real brain geometry (electrode: 0.1, domain: 0.85).

4.2 Simulations

Simulation scenario 1: difference between meshing methods

The relative difference between meshing methods in the homogeneous spherical domain with monopolar stimulation can be seen in figure 9. At the location of the electrode stem of method 2, locally varying differences can be seen. This corresponds to what we have seen in the accuracy of the mesh (figure 6). For the rest of the domain, the influence is most pronounced closer to the electrode contacts.

Scenario 1: difference in E-field for monopolar stimulation

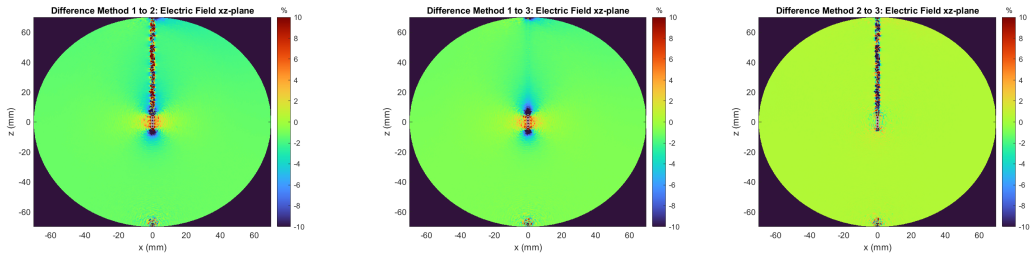

(a) **(b)** **(c)**

Figure 9: Relative difference in E-field of monopolar stimulation on all contacts in spherical domain diameter=140mm in xz-plane a) difference between method 1 and 2, b) difference between method 1 and 3, c) difference between method 2 and 3.

If we analyse the plots in figure 10 we see results corresponding to the visual inspection. A decrease in E-field magnitude can be seen close to the electrode at 10mm. This decrease becomes less pronounced further away from the contacts. From 30mm away, the difference between all methods is consistent. In farther regions, the influence of method two is a decrease of 2%, for method 3 this is 1%. Farher in the domain, the local variation is low, and an even spread in the decrease of E-field is observed in both method 2 and method 3 (10d-f).

Scenario 1: difference in E-field for monopolar stimulation r=10mm-60mm

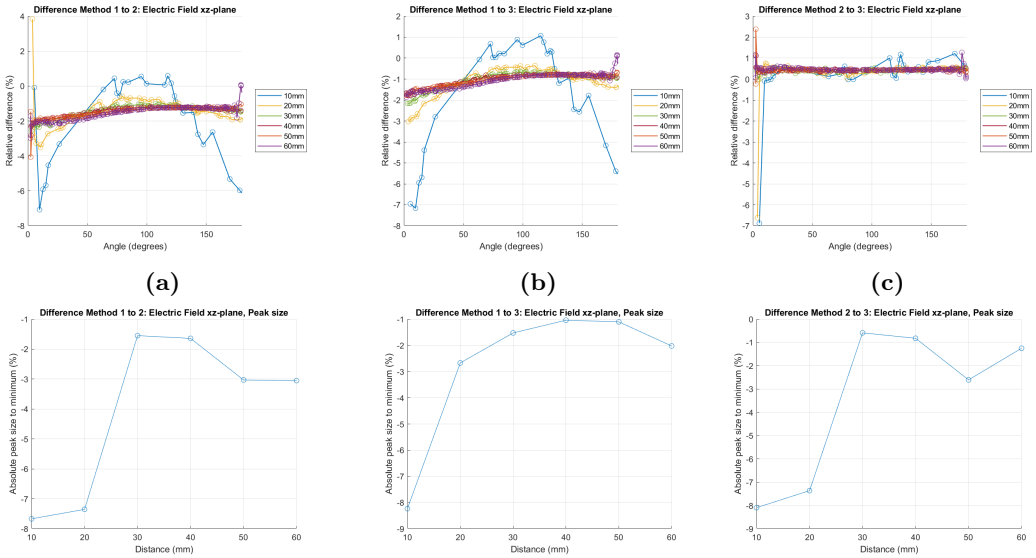

Figure 10: Relative difference in E-field (r=10mm-60mm) of monopolar stimulation on all contacts in spherical domain in xz-plane in plot a) difference between method 1 and 2, b) difference between method 1 and 3, c) difference between method 2 and 3,d) peak size of difference between method 1 and 2, e) peak size between method 1 and 3, f) peak size of difference between method 2 and 3.

Close to the electrode a similar trend is seen (figure 11). At 0°and 180°the difference is highest. Starting at 9mm from the electrode the difference in E-field magnitude becomes more even when going further away. At 5mm from the electrode, we see almost no difference in the E-field magnitude. Note here that the differences close to the electrode insulation are not plotted due to limitations in data resolution.

For monopolar stimulation, comparing method 2 to method 3, we see method 3 reports a 0.5% increase in E-field distances farther than 20mm.

Scenario 1: difference in E-field for monopolar stimulation r=5mm-15mm

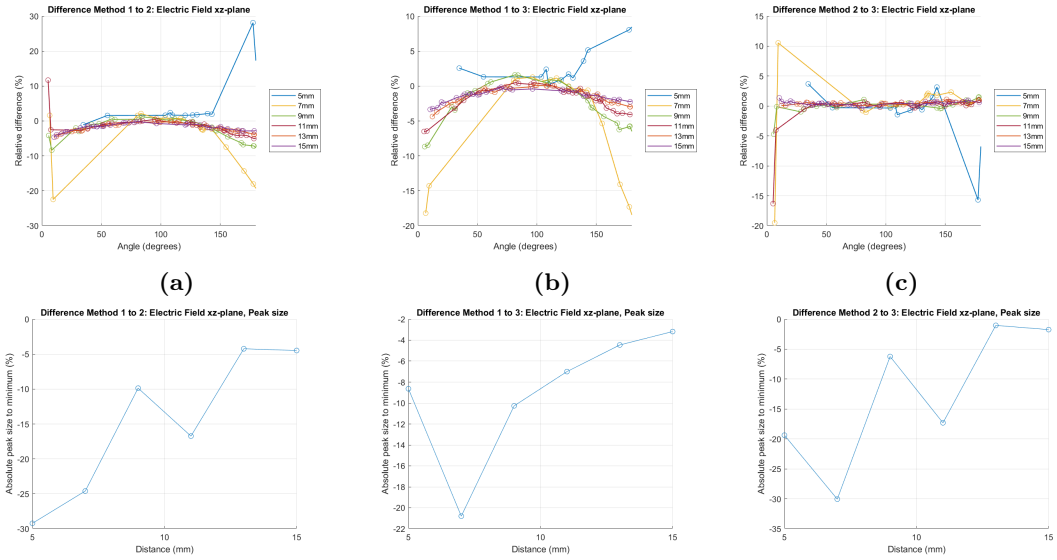

Figure 11: Relative difference in E-field (r=5mm-15mm) of monopolar stimulation on all contacts in spherical domain in xz-plane in plot a) difference between method 1 and 2, b) difference between method 1 and 3, c) difference between method 2 and 3,d) peak size of difference between method 1 and 2, e) peak size of difference between method 1 and 3, f) peak size of difference between method 2 and 3.

The relative difference between meshing methods in the homogeneous spherical domain with bipolar stimulation can be seen in figure 12. At the location of the electrode stem of method 2, locally varying differences can be seen. This corresponds to what we have seen in the accuracy of the mesh (figure 6), and to what we have seen in the monopolar simulation. In the rest of the domain, the influence on the E-field seems to be most impactful closer to the electrode contacts. One exception is at the bottom of the domain, where a large increase in E-field magnitude is seen. This location corresponds to the area around the grounding contact.

Scenario 1: difference in E-field for bipolar stimulation

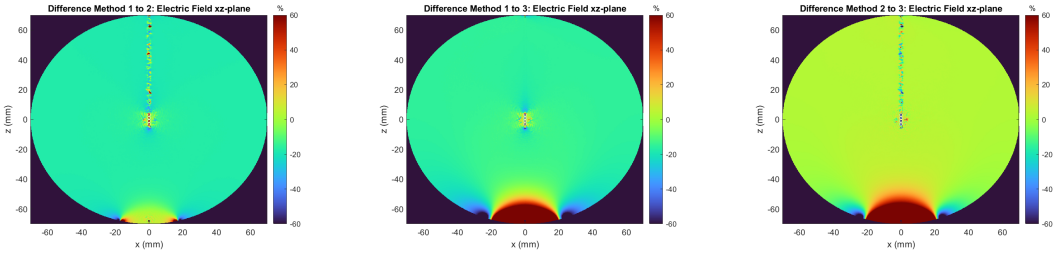

Figure 12: Relative difference in E-field of bipolar stimulation on all contacts in spherical domain in xz-plane a) difference between method 1 and 2, b) difference between method 1 and 3, c) difference between method 2 and 3.

Figure 13 shows results corresponding to the visual inspection. E-field magnitude decreases more than 14% close to the electrode contacts (r=10mm). This decrease becomes less

locally varying farther away from the electrode. From 20mm away, the difference between all methods seems generally consistent. The exception identified visually is also seen here. Spiking to a difference of 100% at r=60mm at an angle of 180°. When we omit this region from the results we can see that bipolar stimulation with method 2 decreases the E-field magnitude at the farther regions by 17%. Method 3 decreases the E-field by around 15%. The local variation for bipolar stimulation follows the same trend as for monopolar stimulation in a homogeneous domain, with an exception locally around the grounding contact.

Scenario 1: difference in E-field for bipolar stimulation r=10mm-60mm

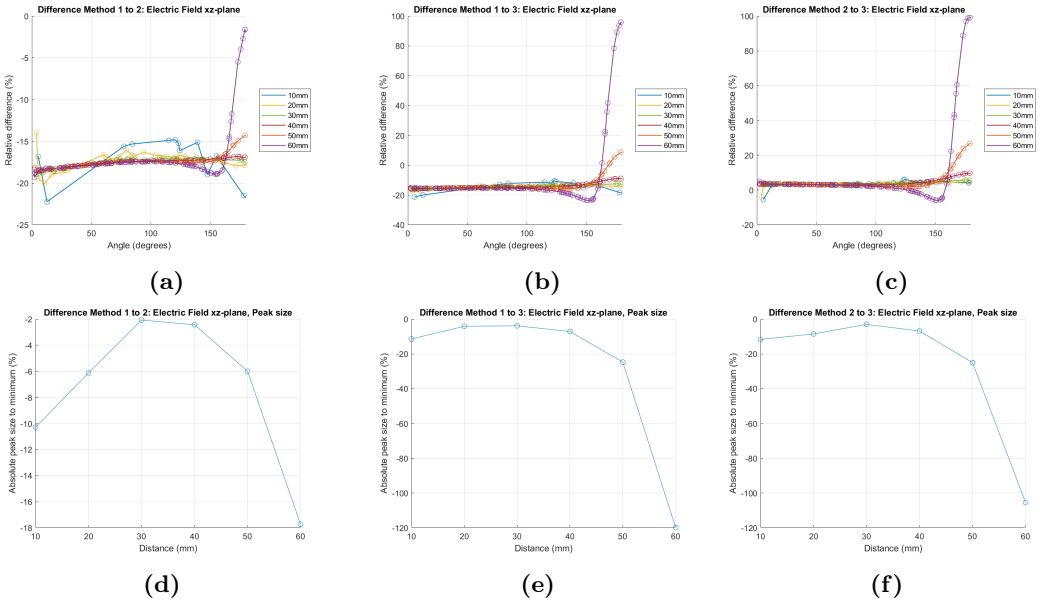

Figure 13: Relative difference in E-field (r=10mm-60mm) of bipolar stimulation on all contacts in spherical domain in xz-plane in plot a) difference between method 1 and 2, b) difference between method 1 and 3, c) difference between method 2 and 3,d) peak size of difference between method 1 and 2, e) peak size of difference between method 1 and 3, f) peak size of difference between method 2 and 3.

Looking closer around the electrode, similar trends as in monopolar stimulation are identified. Closer to the electrode the differences in E-field magnitude become more severe, and more locally influenced. Peaks are observed at 0°and 180°. Again the resolution of the data was not high enough to compare r=5mm from the electrode with the rest of the plots. Finally, comparing method 3 to method 2 shows an increase of E-field of around 4% for most distances.

Scenario 1: difference in E-field for bipolar stimulation r=5mm-15mm

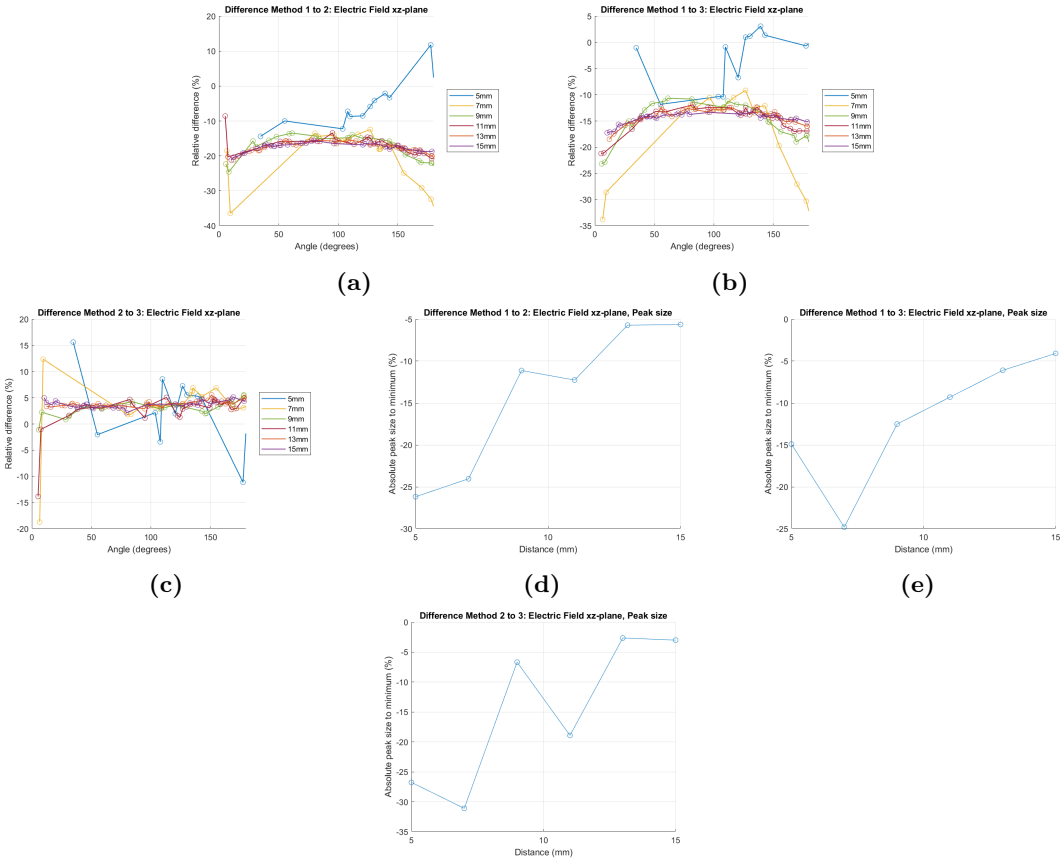

Figure 14: Relative difference in E-field (r=5mm-15mm) of bipolar stimulation on all contacts in spherical domain in xz-plane in plot a) difference between method 1 and 2, b) difference between method 1 and 3, c) difference between method 2 and 3,d) peak size of difference between method 1 and 2, e) peak size of difference between method 1 and 3, f) peak size of difference between method 2 and 3.

Simulation scenario 2: influence insulation in head model

For scenario 2, the electric field and the difference in magnitude for monopolar stimulation can be seen in figure 15.

Method 3 seems to influence the magnitude of the E-field most close to the electrode. The regions where there is a change in conductivity, and which lie close to the electrode insulation (0°), also seem to be affected. However, plots 15a-b indicate that the E-field magnitude in this area is less than 0.01V/m. In this area even a very small change can thus influence the difference as seen in plot 15c).

Scenario 2: E-field for monopolar stimulation

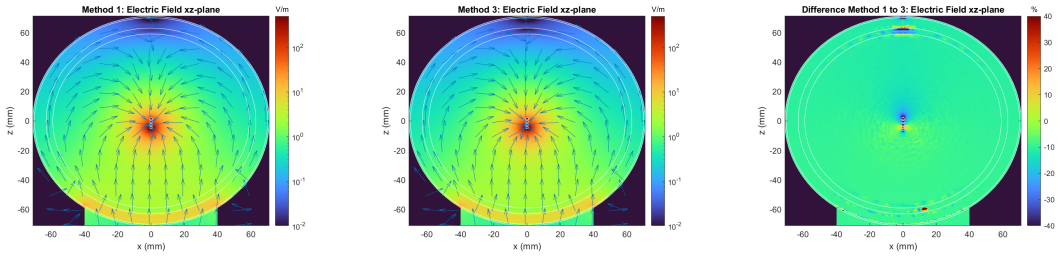

(a) **(b)** **(c)**

Figure 15: Results of monopolar stimulation in head model in xz-plane a) E-field of meshing method 1, b) E-field of meshing method 3, c) relative difference between method 1 and 3.

Close to the electrode (r=10mm), there is a large, localised decrease in E-field, peaking at -30% (figure 16). From 30mm away, the decrease becomes less pronounced and less localised. A difference between scenario 1 and the multi-sphere head model is that for the latter the decrease in E-field is larger as opposed to a homogeneous domain. For regions further away in the domain (r>30mm) the difference in magnitude is around -8%. In scenario 2, the peak values indicate that farther away in the domain, the decrease in magnitude becomes less locally varied. With an exception at 60mm, which is inside the skull region (figure 16b).

Scenario 2: difference in E-field for monopolar stimulation r=10mm-60mm

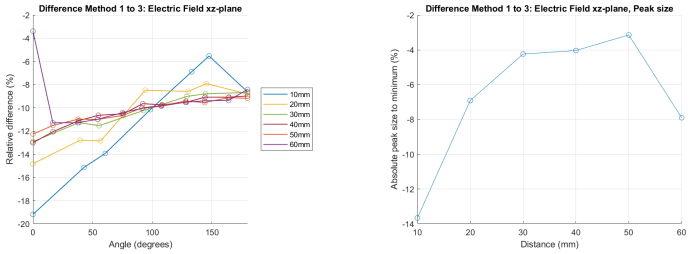

(a) **(b)**

Figure 16: Results of difference (r=10mm-60mm)between methods in monopolar stimulation in plot a) difference in magnitude as a function of angle and distance, b) peak size of the results.

Evaluation of the regions closer to the contacts (r=5mm-15mm) shows the same trends as for the analysis of the larger distances (r=10mm-60mm) (figure 17). Closest to the electrode the difference is most severe, with the electric field magnitude getting decreased more at 0°(-35%)than at 180°. (-14%)

Scenario 2: difference in E-field for monopolar stimulation r=5mm-15mm

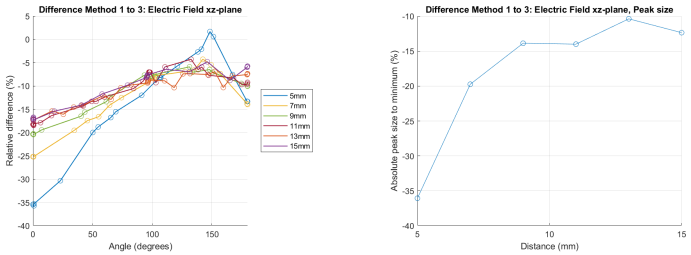

(a) **(b)**

Figure 17: Results of difference (r=5mm-15mm) between methods in monopolar stimulation in plot a) difference as a function of angle and distance, b) peak size of the results.

For bipolar stimulations, the results differ when meshing via methods 1 or 3 (figure 18). When adding the insulation, the E-field becomes contained inside the skull, whereas simulating without insulation shows E-fields travelling towards the neck, where the ground is located. This difference is also seen in figure 18c. The increase in magnitude corresponds to the location where the change in direction of the E-field is observed.

Scenario 2: E-field for bipolar stimulation

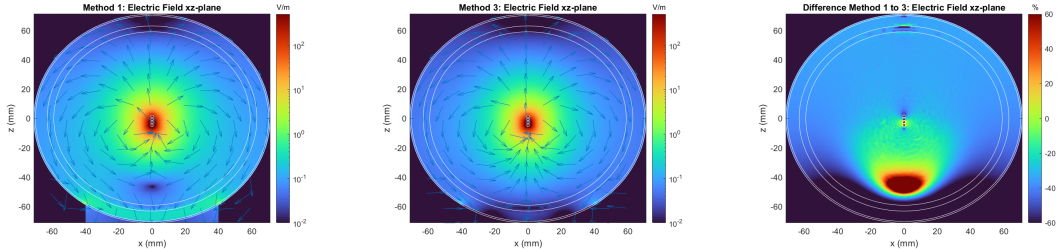

(a) **(b)** **(c)**

Figure 18: Results of bipolar stimulation in head model in xz-plane a) E-field of meshing method 1, b) E-field of meshing method 3, c) relative difference between method 1 and 3.

At r=40mm an increase of 100% is seen (figure 19), corresponding to the location identified in figure 18c. Between distances 40mm to 50mm, the increase becomes less severe, reduced to 20%. From 60mm away, the E-field magnitude decreases again by meshing via method 3.

Scenario 2: difference in E-field for bipolar stimulation r=10mm-60mm

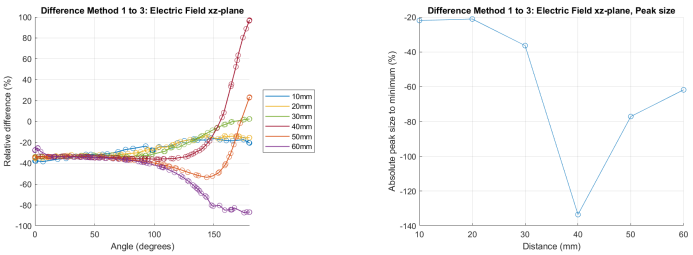

(a) **(b)**

Figure 19: Results of difference between methods (r=10mm-60mm) in bipolar stimulation in plot a) difference as a function of angle and distance, b) peak size of the results.

Closer to the electrode (r<15mm) the same trends as in monopolar stimulation of the head model are observed. Closer to the electrode the Electric field is decreased more, peaking at -50% at 5mm away at 0°(figure 20). The decrease of E-field magnitude is higher towards the stem (-50%) than towards the tip of the electrode (-27%).

Scenario 2: difference in E-field for bipolar stimulation r=5mm-15mm

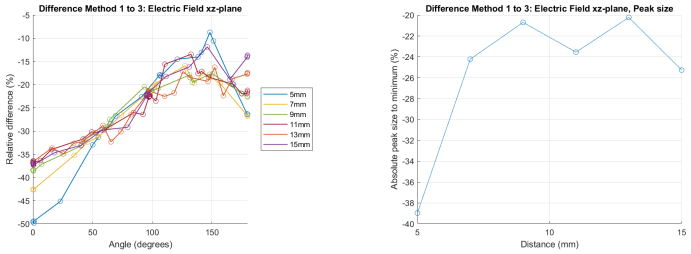

(a) **(b)**

Figure 20: Results of difference between methods (r=5mm-15mm) in bipolar stimulation in plota) difference as a function of angle and distance, b) peak size of the results.

To summarize, comparable trends between monopolar and bipolar stimulation settings for scenario 1 are seen. Close by the electrode r<15mm, the decrease in magnitude is more pronounced than further away. Here, the decrease in magnitude towards 0°and 180°are equal, exhibiting symmetry. Further away in the domain, r>30mm, the change in electric field magnitude becomes less locally varying around the domain. The biggest difference between monopolar and bipolar stimulation is the region around the ground contact in the model. The monopolar stimulation indicates consistent trends as the rest of the domain, whereas bipolar stimulation indicates an increase in magnitude in this area.

Comparing trends between monopolar and bipolar stimulation settings in scenario 2, the comparable trends are obtained. Both stimulation settings show a higher decrease in E-field magnitude closer to the electrode (r<20mm), with peaks at 0°and 180°. In both cases, the decrease in magnitude was higher towards 0°than 180°, exhibiting asymmetry. After 30mm, monopolar and bipolar stimulation change trends. For monopolar stimulation, the decrease in magnitude becomes even around the domain, with small local increases around the insulation at boundaries between materials. The domain has more variation in electric field magnitude for bipolar stimulation. Between 40mm and 50mm, a spike of 100% increase is seen in E-field magnitude. For regions farther than 60mm, the decrease becomes more even. As for monopolar, bipolar stimulation also shows local variation in the influence on the electric magnitude at the crossing of boundaries close to the insulating stem.

The main difference between scenarios 1 and 2 is that the influences on the electric field are more severe for scenario 2. In scenario 2, monopolar stimulation showed at least 8% more decrease in magnitude in scenario 2. Bipolar stimulation showed generally around 20% more decrease in magnitude.

5 Discussion

In this thesis, a new method to incorporate electrode geometry into a brain model was introduced. This method was consequently tested to see the influence on the electric fields as compared to the existing meshing methods.

Results showed a prominent influence in electric field magnitude over the whole domain when adding insulation for both scenarios 1 and 2. For all scenarios, when evaluating areas close to the electrode contacts, adding insulation caused local variation in the difference of E-field magnitude. In farther regions, the E-field was also influenced, but the magnitude had less local variation.
Generally, changes to monopolar stimulation were less severe than those occurring for bipolar stimulation.

Mesh generation

First, the newly introduced meshing method will be discussed, then the simulation results. The biggest drawback of the new method is that refining of the submeshes is needed. The refined mesh has a higher tetrahedral resolution, but also loses some surface geometry compared to the reference mesh. The decrease in electrode surface resolution does not seem to be prevalent enough to impact results severely but might introduce inaccuracies when modelling more complex electrode geometries, especially for the internal boundaries. The refining of the mesh inherently causes the generated meshes to have more tetrahedrons. This will cause more RAM space to be taken up by the meshes and will increase simulation times. In further research local refinement should be implemented to decrease the impact on computing time.

Method 3 was very flexible and robust in mesh generation. It can be argued that method 2 also can introduce the electrode in an arbitrary orientation. This is true, but the drawback is that the electrode contacts still may not cross a boundary. During an inspection of patient data within the DECODE project, it was already discovered there are patients where the electrode contacts cross the boundary between grey and white matter, which will cause problems in mesh generation for method 2.

Simulations

The simulation settings that were used, might have impacted the results. In scenario 1 non-clinical settings were used. In this scenario, all four contacts were used as voltage sources, whereas in clinical settings only one (for monopolar) or two (bipolar) are used. In scenario 2 these clinical parameters were used. The reasoning for this difference in simulation settings was to have scenario 1 be modelled as a worst-case scenario to make the difference between methods more clear. The assumption was that setting more contacts as a source would create more complex electric fields, causing the insulation to exhibit a larger influence. Scenario 2 was designed to simulate an approximation of DBS in a human head. This way scenario 2 would give a more realistic expectation of what could happen when simulation real head geometries. In our results, the opposite happened. Scenario 2 produced more pronounced influences on the electric field than the simulations from scenario 1. In addition, scenario 1 shows a symmetrical influence in magnitude around the electrode whereas scenario 2 shows asymmetrical effects. The differences between scenarios are logically explained. In scenario 2, the electric fields have to pass both the upper contacts and the insulation in between. In scenario 1, both upper and lower contacts radiate. This causes the effect of adding insulation to the simulations to be larger in scenario 2.

Evaluating scenario 1, the difference between methods 2 and 3 showed that more precise meshing of the electrode did not result in a larger difference in electric field, in the worst scenario differing about 5% for most of the domain. It must be noted, however, that refining the insulation for bipolar stimulation caused a prominent local increase in electric field

strength between methods 2 and 3 (+100% at r=60mm for 180°). Monopolar stimulation did not show this. For bipolar stimulation in scenario 2, a similar peak in an increase of electric field strength was observed too (+100% at r=40mm for 180°), but for a different region. This local anomaly is expected to arise from the simulation parameters. When adding insulation, contact 1's lower surface is blocked, causing less E-field to pass through. This is expected to be the underlying cause of these anomalies. To validate this, bipolar stimulation settings must be tested in the whole head model. If a similar local variation is observed, more research has to be done to decide which meshing method creates more valid results. It is expected meshing method 3 is more valid due to the more accurate description of outer electrode geometry.

In scenario 2, differences in the E-field are observed at the boundaries with different conductivities, around the electrode lead. Although these differences are indicated to be relevant by the spikes in peak size, it is not expected that these have any real implications on the efficacy of DBS. The E-field in these regions is lower than 0.01V/m. Research from Francis et al. [21] indicates a neural threshold of 0.295 V/m is needed for modulation.

Comparison to literature

Previous research by Vermaas et al. [12] shows that, when introducing measuring electrodes, it is needed to accurately model electrode impedances if the distance to the electrode is smaller than the electrode diameter. In this thesis, the distance to the main region of interest (the cortex) is larger than the electrode diameter. However, it has been shown that introducing more precise electrode insulation properties has a prominent effect on electric field magnitude in this region. Scenario 2 indicates an expected absolute difference of more than 10% for both monopolar and bipolar stimulation in cortical regions. In the secondary region of interest, the basal ganglia itself, an even larger difference in electric field strength is observed when adding insulation.

Other developments in DBS show a preference for current-controlled stimulation settings over voltage-controlled sources. Current-controlled stimulation reduces fluctuations in the E-field measured in-vivo [22]. Voltage-controlled stimulation is susceptible to changes in material impedances in the domain, causing potential drops. Current-controlled stimulation provides constant potentials over different contact impedances [22]. Especially in clinical settings, current-controlled sources are preferred. The implantation of the DBS-electrode will induce scar tissue around the electrode, and will therefore alter the impedance around the electrode unpredictably.
For the simulations in this thesis, the use of voltage sources is not expected to be a problem. Literature shows that both current-controlled and voltage-controlled sources have been used in the simulation of DBS [23, 24]. Both are expected to give valid simulation results. During this thesis, the source magnitude is kept constant and the area directly around the electrode has a constant impedance. For future work it is recommended to change to current-controlled sources, to represent current clinical practice.

Current limitations

It is shown that the newly introduced meshing method is robust and depicts an accurate description of the electrode surface geometry. The new meshing method still has some limitations that should be addressed. The main point of concern is the inaccuracy of the internal electrode boundaries. These have less accuracy since mesh generation defines the tetrahedron size depending on how close the element is to a boundary. This is also the

reason for the low resolution of electrode domain 5 in method 2, but the relatively good resolution in between the contacts. In method 3, the internal boundaries should be able to be defined better. A course of action can be to introduce a planar mesh and merge this on the location of the electrode boundaries. By removing the excess mesh that would then exist outside the electrode surface, an accurate internal boundary would be created. This would combine the good internal boundary conservation of method 2 with the robust surface geometry and placement possibilities of method 3.

A second limitation of the current script lies within the secondary post-processing step. This step aims to resolve conflicting domains by relabelling elements to the closest neighbour. It limits the possibilities by restricting the ability to relabel to non-electrode domains. The problem arises in the generation of the Ernie brain-electrode mesh. During the merging and refining of the brain mesh, isolated regions are produced within the grey and/or white matter. These get labelled as conflicting domains but do not lie close to the electrode, causing them to not be resolved. This can be fixed by extending the function by first evaluating conflicting domains close to the electrode, and then searching for the isolated domains and relabelling them accordingly.

Combining our results with the findings of Vermaas et al . [12], it is recommended to always model the stimulating electrode as accurately as possible to obtain the most representative results, especially in future work within the DECODE project where different electrode geometries and stimulation parameters might be included. For now, meshing method 3 is recommended. Due to the low conductivity of the insulation, it is expected that the low-resolution boundary between the electrode subdomains has no prominent influence on the simulation results. Still, implementations should be made to counteract the limitations described above.

6 Conclusion

In this thesis, a mesh generation procedure was developed and compared with existing methods. With this new method, it was possible to introduce a DBS electrode inside an arbitrary domain with an arbitrary position. The new method relies on the remeshing of surface geometries and then relabelling the element domains. The new method conserves geometry, but loses some precision as compared to the original reference mesh. The biggest drawback of this new method lies in the low conservation of the boundaries between electrode domains.

Simulations in the homogeneous domain have shown a relevant difference in E-field magnitude between simulating only electrode contacts (method 1) as opposed to simulating with the addition of electrode insulation (methods 2 and 3). The difference between the method based on relabelling domain elements (method 2) and the method developed in this thesis (method 3) was much smaller. Simulations in a four-sphere head model also showed a more prominent difference between modelling electrode geometry without and with insulation.

To conclude, the biggest advantage of the newly introduced meshing procedure is its flexibility in mesh generation. In simulation accuracy, however, the advantage of method 3 over method 2 seems to be less relevant. From simulations in scenario 1, it is seen that the inclusion of any insulation is more important than how accurately this insulation mesh is modelled, especially when evaluating cortical regions. Still, for future simulations within the DECODE project, it is recommended to use the new method over method 2 due to

the robustness of mesh generation. When simulating more complex electrode geometries, it is recommended to expand the new method such that internal electrode boundaries are also geometrically conserved.

References

[1] Ole-Bjørn Tysnes and Anette Storstein. "Epidemiology of Parkinson's disease". In: *J. Neural Transm.* 124.8 (Aug. 2017), pp. 901–905. ISSN: 1435-1463. DOI: 10.1007/s00702-017-1686-y.

[2] Sigurlaug Sveinbjornsdottir. "The clinical symptoms of Parkinson's disease". In: *J. Neurochem.* 139.S1 (Oct. 2016), pp. 318–324. ISSN: 0022-3042. DOI: 10.1111/jnc.13691.

[3] Gabriel E Vázquez-Vélez and Huda Y Zoghbi. "Parkinson's disease genetics and pathophysiology". In: *Annual review of neuroscience* 44 (2021), pp. 87–108.

[4] Dale Purves. *Neuroscience, Ch18: Modulation of movement by the basal ganglia. 5^{th}ed.*. Sinauer Associates, INC, 2012. ISBN: 978-0-87893-695-3.

[5] Thomas B. Stoker and Roger A. Barker. "Recent developments in the treatment of Parkinson's Disease". In: *F1000Research* 9 (2020). DOI: 10.12688/f1000research.25634.1.

[6] Can Sarica et al. "Trends and disparities in deep brain stimulation utilization in the United States: a Nationwide Inpatient Sample analysis from 1993 to 2017". In: *Lancet Regional Health - Americas* 26 (Oct. 2023). DOI: 10.1016/j.lana.2023.100599.

[7] Christian J. Hartmann et al. "An update on best practice of deep brain stimulation in Parkinson's disease". In: *Ther. Adv. Neurol. Disord.* 12 (Jan. 2019), p. 1756286419838096. ISSN: 1756-2864. DOI: 10.1177/1756286419838096.

[8] Morten L. Kringelbach et al. "Translational principles of deep brain stimulation". In: *Nat. Rev. Neurosci.* 8 (Aug. 2007), pp. 623–635. ISSN: 1471-0048. DOI: 10.1038/nrn2196.

[9] Alessandra Del Felice et al. "Personalized transcranial alternating current stimulation (tACS) and physical therapy to treat motor and cognitive symptoms in Parkinson's disease: A randomized cross-over trial". In: *NeuroImage: Clinical* 22 (Jan. 2019), p. 101768. ISSN: 2213-1582. DOI: 10.1016/j.nicl.2019.101768.

[10] Florian H. Kasten et al. "Integrating electric field modeling and neuroimaging to explain inter-individual variability of tACS effects". In: *Nat. Commun.* 10.5427 (Nov. 2019), pp. 1–11. ISSN: 2041-1723. DOI: 10.1038/s41467-019-13417-6.

[11] P.L. de Boeij and C.G. Zeinstra. *Lecture notes in Finite Element methods*. Jan. 2023.

[12] M. Vermaas et al. "When to include ECoG electrode properties in volume conduction models". In: *J. Neural Eng.* 17.5 (Oct. 2020), p. 056031. ISSN: 1741-2552. DOI: 10.1088/1741-2552/abb11d.

[13] COMSOL Inc. *COMSOL Multiphysics 6.1*. 2024. URL: http://www.comsol.com/products/multiphysics/.

[14] Cristian A. Torres-Valencia, Genaro Daza-Santacoloma, and Alvaro A. Orozco-Gutiérrez. "Electric propagation modeling of Deep Brain Stimulation (DBS) using the finite element method (FEM)". In: *2014 XIX Symposium on Image, Signal Processing and Artificial Vision*. IEEE, pp. 17–19. ISBN: 978-1-4799-7666-9. DOI: 10.1109/STSIVA.2014.7010180.

[15] Guilherme B. Saturnino et al. "SimNIBS 2.1: A Comprehensive Pipeline for Individualized Electric Field Modelling for Transcranial Brain Stimulation". In: *bioRxiv* (Dec. 2018), p. 500314. eprint: 500314. URL: https://doi.org/10.1101/500314.

[16] Oula Puonti et al. "Accurate and robust whole-head segmentation from magnetic resonance images for individualized head modeling". In: *Neuroimage* 219 (Oct. 2020), p. 117044. ISSN: 1053-8119. DOI: 10.1016/j.neuroimage.2020.117044.

[17] Andreas Horn and Andrea A. Kühn. "Lead-DBS: A toolbox for deep brain stimulation electrode localizations and visualizations". In: *Neuroimage* 107 (Feb. 2015), pp. 127–135. ISSN: 1053-8119. DOI: 10.1016/j.neuroimage.2014.12.002.

[18] Qianqian Fang and David A Boas. "Tetrahedral mesh generation from volumetric binary and grayscale images". In: *2009 IEEE international symposium on biomedical imaging: from nano to macro*. Ieee. 2009, pp. 1142–1145.

[19] Hang Si. "TetGen, a Delaunay-Based Quality Tetrahedral Mesh Generator". In: *ACM Trans. Math. Software* 41.2 (Feb. 2015), pp. 1–36. ISSN: 0098-3500. DOI: 10.1145/2629697.

[20] Joshua Kahan et al. "The Safety of Using Body-Transmit MRI in Patients with Implanted Deep Brain Stimulation Devices". In: *PLoS One* 10 (June 2015), e0129077. DOI: 10.1371/journal.pone.0129077.

[21] Joseph T. Francis, Bruce J. Gluckman, and Steven J. Schiff. "Sensitivity of Neurons to Weak Electric Fields". In: *J. Neurosci.* 23.19 (Aug. 2003), p. 7255. DOI: 10.1523/JNEUROSCI.23-19-07255.2003.

[22] Scott F. Lempka et al. "Current-controlled deep brain stimulation reduces in vivo voltage fluctuations observed during voltage-controlled stimulation". In: *Clinical neurophysiology : official journal of the International Federation of Clinical Neurophysiology* 121.12 (Dec. 2010), p. 2128. DOI: 10.1016/j.clinph.2010.04.026.

[23] Peadar F. Grant and Madeleine M. Lowery. "Electric field distribution in a finite-volume head model of deep brain stimulation". In: *Med. Eng. Phys.* 31.9 (Nov. 2009), pp. 1095–1103. ISSN: 1350-4533. DOI: 10.1016/j.medengphy.2009.07.006.

[24] Konstantin Butenko et al. "OSS-DBS: Open-source simulation platform for deep brain stimulation with a comprehensive automated modeling". In: *PLoS Comput. Biol.* 16.7 (July 2020), e1008023. ISSN: 1553-7358. DOI: 10.1371/journal.pcbi.1008023.

Appendices

A Simulation Parameters

Table 1: Simulation material properties

Material	Relative Permittivity ε_r	Conductivity σ (S/m)
White matter	1.07E6	5.9E-2
Grey Matter	2.46E6	9.15E-2
Blood/Muscle	5.26E6	2.78E-1
Platinum	1	8.9E6
Insulation	2.3	10E-18

Table 2: Simulation parameters simulation scenario 2

Domain	Material	Boundary condition
c1	Platinum	Electric Potential -2.5V (Bipolar) / +2.5V (Monopolar)
c2	Platinum	Electric Potential +2.5V (Bipolar) / +2.5V (Monopolar)
c3	Platinum	Electric Potential -2.5V (Bipolar) / +2.5V (Monopolar)
c4	Platinum	Electric Potential +2.5V (Bipolar) / +2.5V (Monopolar)
i5	Insulation	Current Conservation
i6	Insulation	Current Conservation
i7	Insulation	Current Conservation
i8	Insulation	Current Conservation
i9	Insulation	Current Conservation
d10	Grey matter	Current Conservation
g11	Platinum	Ground
Boundary	-	Electric Insulation

Table 3: Simulation parameters simulation scenario 2

Domain	Material	Boundary condition
c1	Platinum	Electric Potential -2.5V (Bipolar) / -2.5V (Monopolar)
c2	Platinum	Electric Potential +2.5V(Bipolar) / Current Conservation (Monopolar)
c3	Platinum	Current Conservation
c4	Platinum	Current Conservation
i5	Insulation	Current Conservation
i6	Insulation	Current Conservation
i7	Insulation	Current Conservation
i8	Insulation	Current Conservation
i9	Insulation	Current Conservation
d10	White matter	Current Conservation
d11	Grey matter	Current Conservation
d12	Bone	Current Conservation
d13	Skin	Current Conservation
d14	Blood/Muscle	Current Conservation
g15	Platinum	ground
Boundary	-	Electric Insulation